ACS POLYMERS Au
AN OPEN ACCESS JOURNAL OF THE AMERICAN CHEMICAL SOCIETY

pubs.acs.org/polymerau
Article

Effect of Polymer Gel Elasticity on Complex Coacervate Phase Behavior

Published as part of ACS Polymers Au virtual special issue "2023 Rising Stars".

Kathryn G. Wilcox, Kai R. Yamagami, Brittany K. Roopnarine, Adam Linscott, and Svetlana Morozova*

Cite This: *ACS Polym. Au* 2024, 4, 109−119
Read Online

ACCESS | Metrics & More | Article Recommendations | Supporting Information

ABSTRACT: Gels are key materials in biological systems such as tissues and may control biocondensate formation and structure. To further understand the effects of elastic environments on biomacromolecular assembly, we have investigated the phase behavior and radii of complex coacervate droplets in polyacrylamide (PAM) networks as a function of gel modulus. Poly-L-lysine (PLL) and sodium hyaluronate (HA) complex coacervate phases were prepared in PAM gels with moduli varying from 0.035 to 15.0 kPa. The size of the complex coacervate droplets is reported from bright-field microscopy and confocal fluorescence microscopy. Overall, the complex coacervate droplet volume decreases inversely with the modulus. Fluorescence microscopy is also used to determine the phase behavior and concentration of fluorescently tagged HA in the complex coacervate phases as a function of ionic strength (100−270 mM). We find that the critical ionic strength and complex coacervate stability are nonmonotonic as a function of the network modulus and that the local gel concentration can be used to control phase behavior and complex coacervate droplet size scale. By understanding how elastic environments influence simple electrostatic assembly, we can further understand how biomacromolecules exist in complex, crowded, and elastic cellular environments.

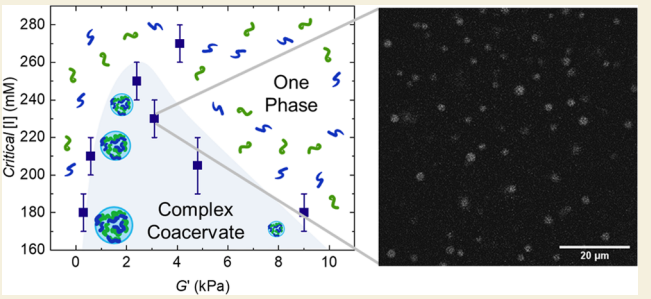

KEYWORDS: *polyelectrolyte complex coacervates, hydrogels, elasticity, phase diagram, phase behavior*

INTRODUCTION

In biological systems, self-assembly typically takes place in crowded, elastic environments.[1−4] Phase separation is one way in which these systems can organize, and biological condensates have recently gained attention as a way to understand biological function and origin of life, and to engineer new biomedical systems.[5−8] Complex coacervates are thought to be similar to these condensates, as complex coacervates are liquid phases that form from the assembly of two oppositely charged polyelectrolytes. As this assembly takes place in elastic environments, understanding the influences of local osmotic stresses and the presence of the networks is necessary to characterize changes in complex coacervate phase behavior.

Complex coacervates are formed from the liquid−liquid phase separation as a result of electrostatic interactions. The resulting bulk, polymer-rich phase has a variety of applications in food additives, personal care products, emulsifiers, drug delivery vehicles, and underwater adhesion.[7,9,10] Complex coacervates have also been studied as models for membraneless organelles[5,11,12] and protocells,[13−16] and used to encapsulate proteins.[17] In biological systems, however, many biocondensates are stable droplets that maintain distinct sizes. To enrich the application space and better understand biological systems, there have been efforts to understand polymer complexation in the context of biology and what factors stabilize complex coacervate phases as stable droplets.[9,10,18−21]

Complex coacervation occurs due to electrostatic interactions, and therefore, the ionic environment has been explored as one method to control the phase behavior. Previous studies have investigated the effects of ionic strength, salt types, charge density, and small molecules on the complex coacervate stability.[7,9,11,22−30] In low ionic strength environments, complex coacervation is strong, but above a critical salt concentration, these phases typically dissolve due to salt screening.[7,31,32] This can result in a range of dense precipitate phases to more dilute liquid complex coacervate phases as a function of the ionic strength. The phase behavior is incredibly

Received: September 15, 2023
Revised: December 7, 2023
Accepted: December 11, 2023
Published: December 26, 2023

rich, and due to the backbone and valency effects, intricate behaviors are observed. Biological polyelectrolytes have trends similar to those of synthetic systems. Li et al. found that the composition of complex coacervate phases formed by poly-L-lysine/poly-L-glutamic acid (PLL/PGA) was significantly influenced by salt concentration.[22] This salt dependence has also been observed in hyaluronic acid and chitosan mixtures.[33] This phenomenon has been generally understood using the Voorn Overbeek prediction,[34] which expands Flory−Huggins theory to include the Debye−Huckle approximation to the enthalpic term. However, many systems have been found to be more complex,[22] including PLL/PGA complex coacervation, and that the salt ion partitioning between the solution and the complex coacervate phase and salt stability can be extremely sensitive to excluded volume effects. Since electrostatic interactions drive complex coacervation, phase separation in the majority of simple salt systems is prevented at higher ionic strengths due to entropic and screening effects.

Polymer crowding has also been shown to affect complex coacervate formation.[35,36] Park et al.[37] found that the addition of polyethylene glycol (PEG) to solutions of ε-poly-L-lysine and hyaluronic acid increased the stability of complex coacervate phases to salt and heightened temperatures. Crowding agents have been predicted to generally expand the phase diagram and increase the salt stability when not participating in the complex coacervate phase.[38] Marianelli et al.[39] investigated the crowding effects of Ficoll, a hydrophilic polysaccharide, and PEG on a polyuridylic acid/spermine phase, which decreased both the minimum complex coacervation concentration of spermine and the total volume of the liquid−liquid phase. Lemetti et al.[40] also found that a dextran crowding agent decreased the concentration of a triblock silk-like fusion protein needed to self-coacervate. In short, crowding effects can improve the physical stability of complex coacervate phases while expanding the range of temperatures, polyelectrolyte concentrations, and ionic strengths at which they can form and exist.

Complex coacervate phases can be stabilized to form droplets with different morphologies. Gao and Srivastava found that a comb polyelectrolyte of poly(acrylic acid)-*graft*-PEG produced microdroplets and increases the stability of poly(acrylic acid sodium salt)/poly(diallydimethylammonium chloride) complex coacervates for over 4 months.[41] Other mixtures have also led to stabilization, including complex coacervates and proteins.[42,43] Based on the structure of the polymers, including diblock and triblock copolymer complex coacervates, morphologies here varied from clusters, to networks, to phase inverted spheres, and even to Janus structures.[44−46] Characterizing the stability of complex coacervate phases is important for understanding how droplet size, morphology, and composition can be locally controlled.

In a recent study, Dufresne et al. found that gel networks can influence the size scale of simple liquid phase separated droplets and hypothesized that local elastic properties of the gel network strongly contributed to this effect.[5,47−52] Style et al. postulate that the droplets grow freely until the droplets reach the network mesh size, after which the droplets deform the network.[53] This results in local cavitation, which can be described by relating the pressure inside the network

$$P = \frac{2\tau}{R} + P_c \tag{1}$$

where τ is the surface tension of the droplet, R is the radius of the droplet, and P_c is the compressive stresses from the polymer network.[54−59] These effects have been shown to lead to droplet migration from higher-modulus areas in the gel to lower-modulus regions and have been termed as "elastic ripening." Rosowski et al. found that elastic ripening can be substantial enough to even reverse Ostwald ripening.[59] Using a similar system, Kim et al. grew, shrank, and regrew elliptical droplets and found the droplets were more elongated after regrowth, indicating that the gel had sustained damage. The damage was distributed around the cavity surface and is consistent with cavitation theory as the droplet size and shape were still limited by the original, remaining gel network.[60] Recently, cavitation has also been found to occur when small liquid phases separate inside fibrous networks[61] and that the deformation results in aspherical morphologies. Biswas et al. developed a mean-field free-energy model for the phase separation of a mixture inside of a polymer gel to predict droplet size as a function of interfacial tension, moduli of the gel, and polymer interactions via the Flory parameter.[62] These seminal results have established that local elastic stresses can control and stabilize liquid-separated droplets based on cavitation. In biological systems, however, and in particular for complex coacervate phases, surface tension is small, and the polymers that make up the network may be miscible in the complex coacervate phases. This presents new opportunities to study a novel class of phase separation inside elastic networks that are directly relevant to biological systems.

Although biological condensates have been extensively studied, their formation and persistence in high salt, crowded, and elastic environments remain largely unknown. To determine how elastic networks affect the phase behavior of complex coacervates, we have investigated the size scale and stability of PLL and HA phases in polyacrylamide networks as shown in Figure 1. Bright-field and confocal fluorescence microscopies were used to image the complex coacervate within the gel network. The size scale and phase behavior are then related to the modulus and concentration of the surrounding network in small-amplitude oscillatory shear experiments. We observe complex coacervation in the form of droplets when phase separation occurs in the gel network, and that droplet volume decreases with increasing gel modulus. We also probe how the modulus of the network changes the complex coacervate phase behavior by determining the HA concentration in the droplets as a function of the ionic

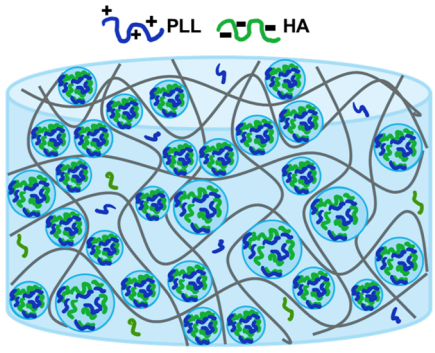

Figure 1. Poly-L-lysine/sodium hyaluronate (PLL/HA) complex coacervates in a polyacrylamide gel. Note: complex coacervate droplet size and the mesh size of the network are not to scale.

https://doi.org/10.1021/acspolymersau.3c00027
ACS Polym. Au 2024, 4, 109−119

Table 1. Acrylamide and Bisacrylamide Ratios for Gel Synthesis, the Resulting Equilibrium Polyacrylamide Gel Concentration, c_e, and Gel Mesh Size[a]

name	acrylamide (%)	bis(acrylamide) (%)	acrylamide stock (mL)	bis(acrylamide) stock (mL)	100 mM sodium acetate (mL)	c_e (mg/mL)	mesh size (nm)
A5B.1	5	0.1	0.625	0.250	4.130	9*	47
A8B.1	8	0.1	1.000	0.250	3.750	13*	35
A8B.25	8	0.25	1.000	1.000	3.000	13*	35
A12B.25	12	0.25	1.500	0.625	2.875	51*	14
A15B.75	15	0.75	2.000	2.000	1.000	52	19
A16B1.2	16	1.2	2.000	3.000	0	115	8
A20B1	20	1	2.500	2.500	0	71	11

[a] c_e values with an * indicated that the concentration was extrapolated using $c_e = (G'/0.51)^{1/2}$.

strength. These findings provide exceptional insights into biomacromolecules that exist in complex, crowded, and elastic cellular environments.

MATERIALS AND METHODS

Materials

Poly-L-lysine hydrobromide (PLL) (M_W = 15,000−30,000 g/mol) and sodium hyaluronate (HA) (M_W = 10 000 g/mol) were purchased from Sigma-Aldrich and Lifecore Biomedical, respectively. For gel synthesis, acrylamide, *N*,*N*′-(1,2-dihydroxyethylene)bis(acrylamide), and 2-hydroxy-4′-(2-hydroxyethoxy)-2-methylpropiophenone were purchased from Sigma-Aldrich. Linear polyacrylamide (PAM) (M_n >150,000 g/mol) was purchased from Sigma-Aldrich, and its M_W = 400,000 as determined from Zimm analysis from static light scatting (see the Supporting Information for more details). Solutions were made by combining deionized water from a Milli-Q Direct 8 system with a resistivity of 18.2 MΩ·cm and sodium acetate from Sigma-Aldrich. For the radius and modulus studies, 100 mM sodium acetate solutions were used. For ionic strength studies, varying amounts of sodium chloride were added to 100 mM sodium acetate solutions to attain final molarities of 150−300 mM solutions. For pH studies, solutions ranging from pH 2 to 5 were prepared by adding concentrated hydrogen chloride dropwise while monitoring the pH with a pH meter. Dilute sodium hydroxide was added dropwise when the pH went below the target pH to achieve the target pH ± 0.02.

Gel Synthesis

The modulus of the polyacrylamide gels was controlled by changing the ratio between the monomer acrylamide and cross-linker *N*,*N*′-(1,2-dihydroxyethylene)bis(acrylamide) in a procedure similar to that of Sheth et al.[63] The full list of ratios used can be found in Table 1. A pregel solution was made by mixing 40% by mass acrylamide and 0.5% by mass *N*,*N*′-(1,2-dihydroxyethylene)bis(acrylamide) in 100 mM sodium acetate solution, as illustrated in Figure S1. 8 mg/mL photoinitiator, 2-hydroxy-4′-(2-hydroxyethoxy)-2-methylpropiophenone was then added, and the solution was filtered using a 0.45 μm PES syringe filter from MDI. Directly prior to gelation, 5 mg of PLL was dissolved into 500 μL of solution and placed in a silicone mold with a 16 mm diameter and 2 mm thickness. To gel, the solution was irradiated for 30 min using a 365 nm wavelength 6-W ultraviolet (UV) lamp. After the gel formed, the gel was soaked in 10 g/L sodium hyaluronate, 100 mM sodium acetate solution for 2 days. In the gel, poly-L-lysine and sodium hyaluronate form the complex coacervate droplets. The gels typically swell after soaking in the HA solution. The volume change of a gel was determined by removing as much excess water as possible from the gel with a Kimwipe and measuring the mass of the gel before and after soaking.

To measure the equilibrium concentration of the PAM of each gel, each gel was first formed from UV exposure. Then, the resulting soft solids were soaked in 100 mM sodium acetate for 2 days to reach swelling equilibrium, after which the mass of the hydrated gel was measured. Each gel was then soaked in deionized water for 2 days and then dried at 85 °C, and the dry mass of the gel was measured. The equilibrium PAM concentration was then calculated by dividing the dry mass by the volume of the hydrated gel where we assumed the density is 1 g/L. The resulting equilibrium PAM concentrations are tabulated in Table 1.

Fluorescently Tagging HA

A 10 mg portion of HA, 200 μL of 0.5 mg/mL tetramethylrhodamine cadaverine purchased from Invitrogen, and 20 mg of 4-(4,6-dimethoxy-1,3,5-triazin-2-yl)-4-methylmorpholinium chloride (DMTMM) purchased from Sigma-Aldrich were mixed in 800 μL of DI water. The solution was placed in an oven at 85 °C for 30 min and then stored in ambient and dark conditions overnight. The solution was then filtered using a 5 kDa molecular weight cutoff Spin-X UF concentrator spin columns from Corning at 13,400 rpm for three sets of 30 min, adding DI water between each set. The solution is diluted back to 10 g/L HA and stored in the freezer until use. To have tagged HA inside the complex coacervate, 100 μL of the tagged HA solution was added to 2500 μL of 10 g/L untagged HA prior to soaking.

To determine the diffusion of HA within the gel, 1 mL of 10 mg/mL HA in DI water, 100 uL of 1 mg/mL AZDye 488 Cadaverine purchased from Vector Labs in DI water, and 50 mg of DMTMM are mixed. The solution was placed in an oven at 80 °C for 40 min and then stored in ambient and dark conditions overnight. The solution was then filtered using a 5 kDa molecular weight cutoff Spin-X UF concentrator spin columns from Corning at 13,400 rpm for three sets of 30 min, adding DI water between each set. The solution was stored in a freezer until use. For the critical ionic strength study, to have tagged HA inside the complex coacervate, 100 μL of the tagged HA solution was added to 2500 μL of the 10 g/L untagged HA prior to soaking. For the HA diffusion study, 250 μL of the tagged HA solution was added to 2500 μL of 10 g/L untagged HA prior to soaking. For the HA diffusion study, the settings that were used are gain 1200, pinhole size 250 μm, and absorption range 500−550 nm.

Bright-field and Confocal Fluorescence Microscopies

For imaging, each soaked gel was placed on a clean glass cover slide. A 63× objective was used for both bright-field and confocal microscopies, and a 100× objective was also used for confocal microscopy. The bright-field images and the confocal images were processed using ImageJ. Complex coacervate regions were manually selected, and the radius of the complex coacervate droplet was calculated from the area, assuming the complex coacervate droplet cross section to be a perfect circle.

The confocal images were taken at the following settings: laser wavelength of 532 nm, laser intensity of 20%, emission of 540−590 nm, gain of 1200, and pinhole diameter of 75 μm. Calibrations were performed to find the HA concentration from the intensity values. Specifically, 20 μL of 0, 1.25, 2.5, 5, and 10 g/L HA were imaged using confocal microscopy with the same settings as the gel samples. The slope of the intensity was plotted against the concentration data (see the SI), along with the tagged/untagged mixing ratio, and is used to calculate the HA concentration in the complex coacervate from the intensity of the complex coacervate droplets. To note, the same tagged HA over the 2 months for the critical ionic strength study and

https://doi.org/10.1021/acspolymersau.3c00027
ACS Polym. Au 2024, 4, 109−119

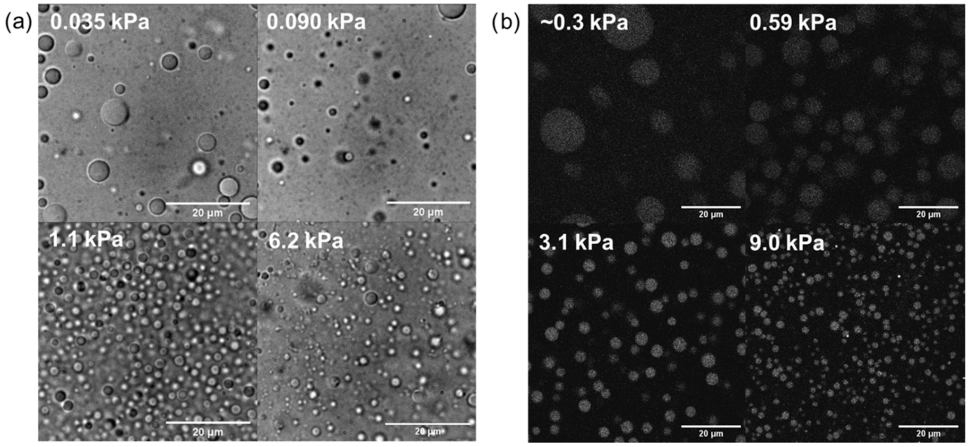

Figure 2. Microscopy images of complex coacervate droplets. (a) 63× bright-field images of complex coacervate droplets in gels with varying moduli from 0.035 to 6.2 kPa and (b) 100× confocal images of complex coacervate droplets in gels with varying moduli from ~0.3 to 9.0 kPa.

photobleaching may have occurred over time for dye, resulting in a slight change in overall intensity.

Solution Study

10 g/L PLL and 10 g/L HA in 100, 150, 200, 250, and 300 mM sodium acetate solutions were combined as a control in solution. To represent the possible range of PLL/HA stoichiometry inside the network, HA and PLL solutions were mixed in two threshold proportions where one extreme assumes no PLL escapes the gel (4.45 g/L PLL:8.30 g/L HA), and the other extreme assumes that PLL exits freely from the gel and equilibrates with the soaking solution (1.48 g/L PLL:8.52 g/L HA). These proportions are based on 450 μL of 10 g/L PLL in the gel. The gel subsequently swells in the 2.6 mL of 10 g/L HA soaking solution by 550 μL for the softest gels. If minimal PLL leaves the gel, due to swelling, the resulting concentration is 4.45 g/L. If PLL fully equilibrates in the solution, the concentration in the gel is reduced to 1.48 g/L. We assume that in all cases as much HA as possible partitions into the network. Another composition (4.45 g/L PLL:5.65 g/L) was also used to further investigate the role of the ratio of HA and PLL in the complex coacervate phase. In addition, PLL and HA were mixed in the presence of 70 g/L linear PAM (M_n = 150,000 g/mol) to investigate crowding effects of PAM without elastic effects of the gel network using 4.45 g/L PLL:8.30 g/L HA and 1.48 g/L PLL:8.52 g/L HA compositions. The actual range of concentrations in the gel is unknown and likely varies depending on the cross-linking density. The charge ratios of the PLL/HA proportions were also calculated where 4.45 g/L PLL:8.30 g/L HA has a charge ratio of 1.39, 4.45 g/L PLL:5.65 g/L HA has a charge ratio of 2.04, and 1.48 g/L PLL:8.52 g/L HA has a charge ratio of 0.45.

Shear Rheology

Oscillatory frequency sweep measurements were taken with a Thermo Fisher Scientific HAAKE MARS III rheometer at a small strain amplitude (γ = 5%) in the frequency (ω) range of 1 to 10 rad/s to determine the modulus of the gels. Measurements were obtained using a 20 mm parallel plate geometry on a Peltier Plate system set to 20 °C. Gap height varied between 1.2 and 2 mm as gel heights between samples varied by the extent of swelling. The modulus of the ~0.3 kPa was not measured from rheology but is extrapolated from all of the other experiments.

RESULTS AND DISCUSSION

Using bright-field and confocal fluorescence microscopies, we have determined the radius and phase behavior of PLL/HA complex coacervate droplets formed in polyacrylamide gels. Oscillatory frequency sweep measurements were used to determine the gel modulus. The droplet HA concentration and salt dependence in the gel network was measured as a function of ionic strength and gel modulus in equilibrium. We observe that the local gel concentration and modulus influence the complex coacervate phase behavior in a nonmonotonic way and that the phase behavior is remarkably different without the gel.

To create the complex coacervate phases inside polyacrylamide networks, a 450 μL PAM gel with 10 g/L PLL is soaked in 2.6 mL of 100 mM sodium acetate, 10 g/L HA solution for 2 days. In Figure 2, bright-field (Figure 2a) and confocal fluorescent (Figure 2b) images of the complex coacervates in the gels are shown. We observe that the complex coacervate droplet radius decreases with increasing gel modulus from 0.035 to 6.2 kPa. To increase the resolution, the droplets were imaged by fluorescence confocal microscopy. HA was tagged with tetramethylrhodamine cadaverine, such that the complex coacervate phase with more concentrated HA is visible against the gel background, with the dilute HA. With higher resolution, and lower background intensity, the confocal images clearly show the size decrease as a function of network modulus in equilibrium from ~0.3 to 15.0 kPa.

The radius was calculated from the area of each droplet, assuming that it is a perfect circle. For both the bright-field and confocal data, the radius decreases with the gel modulus as a power law with exponent −0.3 (Figure 3). The power law fits are shown in Figure 3 and capture the data within error. There

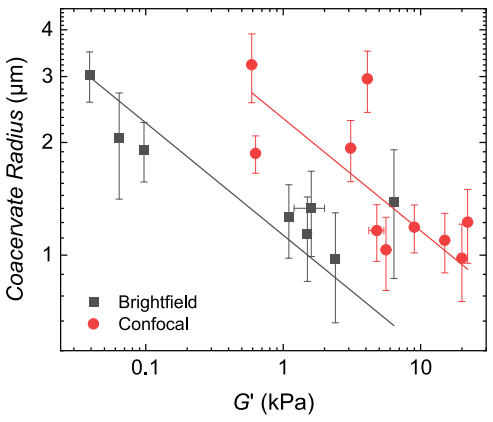

Figure 3. Average complex coacervate droplet radius as a function of the shear modulus of the polyacrylamide gel. Error bars indicate the standard deviation.

https://doi.org/10.1021/acspolymersau.3c00027
ACS Polym. Au 2024, 4, 109−119

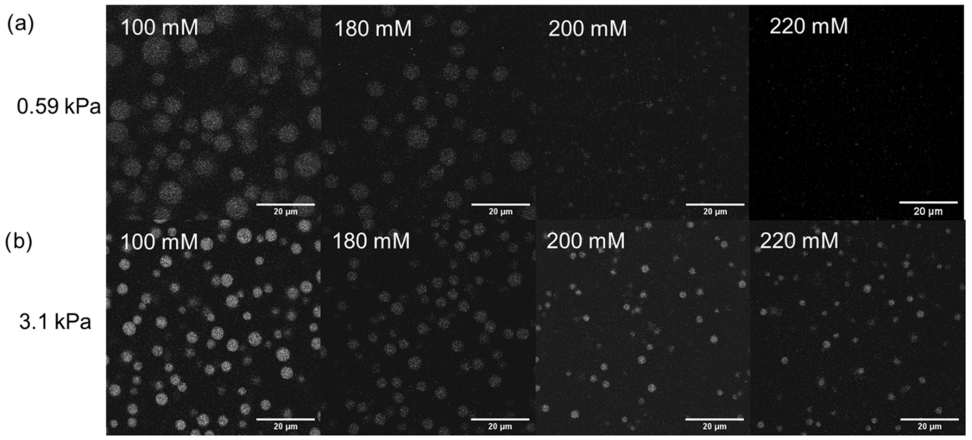

Figure 4. 100× confocal images of complex coacervates with varying ionic strength from 100 to 220 mM for (a) 0.59 kPa PAM gel and (b) 3.1 kPa PAM gel.

is a plateau at high modulus values as the resolution limit is approached. We find that the size is larger when measured with confocal microscopy than with bright-field for the same gels, and this is due to the depth of image and resolution of these methods. The trend indicates that the droplet volume has an inverse relationship with the gel modulus, which differs from previous studies on simpler liquid−liquid phase separation in elastic networks, which show that the droplet radius has an inverse relationship with gel modulus and is set by cavitation.[58,59]

To determine how the surrounding network affects the stability and phase behavior of the HA/PLL complex coacervate droplets, we measured the concentration and critical ionic strength of the phases. It is known that at some critical ionic strength complex coacervation is no longer favorable due to salt screening and entropic effects. First, complex coacervates were formed in gels in 100 mM sodium acetate, which is the buffer used during gelation. Then, each gel was soaked at subsequently higher salt concentrations at 10 mM increments for 2 days to equilibrium. For example, after the gel with complex coacervates was prepared and imaged, the gel was then soaked in a 180 mM sodium acetate solution and then a 190 mM sodium acetate solution. The increase in ionic strength and the soaking process was repeated until droplets were no longer observed in multiple locations throughout the gel. However, it is possible that the complex coacervates still exist but only in very low volumes beyond this ionic strength. As a control, a gel was allowed to soak in only 100 mM for the same amount of time, and no measurable change was observed. Figure 4 shows typical micrographs of the interior of two gels, swollen in ionic strength ranging from 100 to 220 mM. Figure 4a shows a softer 0.59 kPa gel, and Figure 4b shows an intermediate 3.1 kPa gel. The complex coacervate size decreases as the ionic strength increases for both gels. At 220 mM, the droplets were no longer observed in the 0.59 kPa gel, but are still present in the 3.1 kPa gel.

The phase behavior of complex coacervate droplets in gels is summarized in Figure 5. The average droplet radius generally decreases or is stabilized to a certain value as the ionic strength increases for each gel (Figure 5a). For the ∼0.3 kPa gel, the radius decreases from 4.8 to 1.0 μm in the ionic strength range of 100−180 mM, until complex coacervate droplets are no longer apparent at 190 mM. For the 0.59 kPa gel, the radius decreases from 3.2 to 1.0 μm in the [I] = 100−210 mM range,

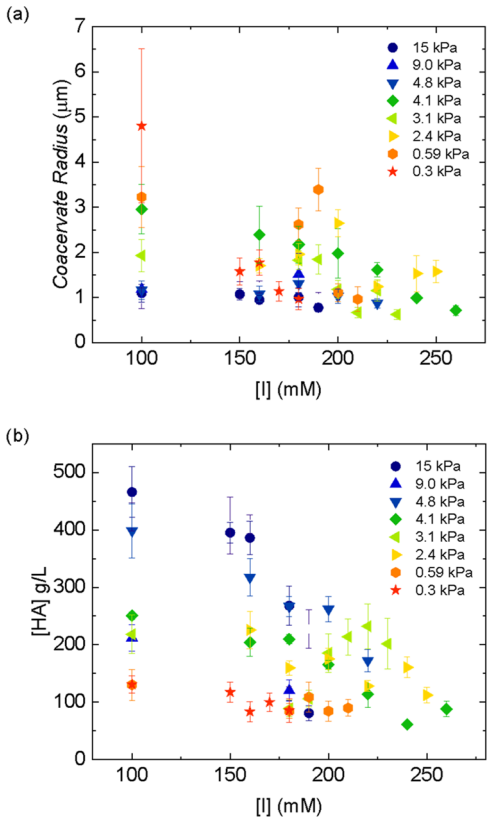

Figure 5. (a) Average complex coacervate radius inside gels of varying moduli as a function of the ionic strength. Error bars indicate standard deviation. (b) Average HA concentration of the complex coacervate droplets inside of gels of varying moduli as a function of the ionic strength. Error bars indicate standard deviation from more than 30 coacervate droplets selected from 3 to 5 images.

until complex coacervate droplets are no longer apparent at 220 mM. For the 3.1 kPa gel, the decrease is 1.9−0.6 μm from 100 to 230 mM, and droplets are no longer observed at 240 mM. For the 4.1 kPa gel, the radius decreases from 3.0 to 0.7 μm as ionic strength changes from 100 to 260 mM, until complex coacervate droplets are no longer apparent at 270 mM. For the 9.0 kPa gel, the complex coacervate droplet radius remained nearly constant within 1.2−1.5 μm in all ionic strengths and dissolved at 190 mM. Similarly, the complex

https://doi.org/10.1021/acspolymersau.3c00027
ACS Polym. Au 2024, 4, 109−119

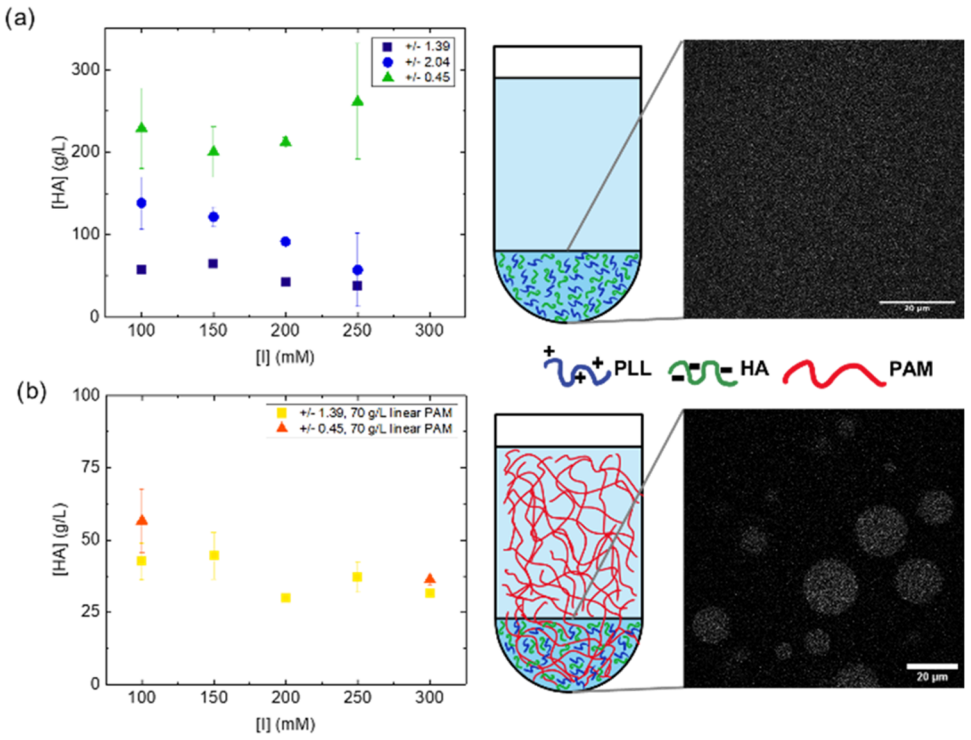

Figure 6. Average HA concentration inside complex coacervates in a bulk phase without linear PAM (a) and with linear PAM (b) and with varying PLL and HA charge ratios as a function of the ionic strength. The confocal microscopy images shown are from the 1.39 charge ratio in 200 mM sodium acetate solution. Error bars represent the standard deviation from duplicate experiments for the charge ratio of 2.04 and triplicate experiments for the charge ratio of 0.45. The charge ratio of 1.39 and all PAM results are from a single experiments, and the error bars represent the standard deviation found between images.

coacervate droplet radius inside of a 15 kPa gel remained nearly constant around ∼1 μm until dissolution at 200 mM. Generally, the decrease in the droplet size is inversely proportional to gel modulus in a constant range of ionic strengths, indicating a balance between the gel strength and complex coacervation strength.

In 100 mM sodium acetate solutions, the HA concentration in the complex coacervate droplets increases as a function of gel modulus. Each HA concentration was calculated from a standard curve that relates the average intensity of the tagged HA to the local HA concentration in the complex coacervate with the imaging settings kept constant (Figure S2). In ∼0.3 and 0.59 kPa gels, the HA concentration is ∼130 g/L, and in higher-modulus gels, the HA concentration increases to ∼470 g/L. The gel has a densifying effect in the complex coacervate phase similar to the results found in Park et al.'s work[37] where PEG was used as a crowding agent. Park et al. found that the concentration of HA and PLL increased by a factor of 1.7 when 3.3 g/mL PEG was added at 100 mM sodium acetate, pH 5 solutions. Overall, with an increase of the gel network modulus and therefore concentration, the HA concentration in the complex coacervate phase increases.

The HA concentration in the droplets decreases monotonically as a function of ionic strength except in the 2.4 and 3.1 kPa gels (Figure 5b). This may indicate that small changes in local network concentration result in large stability changes. For the two softest gels (0.3−0.59 kPa), the concentration decreases from ∼130 to 90 g/L across the ionic strength range. For the highest modulus gels (9−15 kPa), concentration decreases from 210 to 120 g/L and from 470 to 80 g/L, respectively. For the 3.1 kPa gel, the HA concentration decreases from 220 g/L in 100 mM to 90 g/L in 180 mM, and increases back to 190 g/L in 200 mM and stays high until the critical ionic strength of 240 mM.

Solution Study

Electrostatic interactions of oppositely charged polyelectrolytes form complex coacervates as a polymer-rich phase separates from a polymer-poor phase. Without further environmental effects, these two phases exist as two bulk layers. The complex coacervate phase behavior in polyacrylamide gels is considerably different without the presence of a gel. The bulk solution critical ionic strength is 250 mM and is greater than most of the critical ionic strengths found for the complex coacervate phases within the gels.

In order to compare the bulk solution behavior of PLL and HA to their behavior in a gel, we mixed HA and PLL in different ratios in solution. In Figure 6a, we show the variability of the HA concentration inside the bulk solution complex coacervate layer as a function of the charge ratio. In all mixtures, the solution is separated into two distinct phases. For the 4.45 g/L PLL:8.30 g/L HA composition with a charge ratio of 1.39, the concentration of HA in the complex coacervate is lower in solution than in the gel. For the intermediate composition (4.45 g/L PLL:5.65 g/L HA with a charge ratio of 2.04), HA concentration decreases from 138 ± 31 g/L in 100 mM to 57 ± 45 g/L in 250 mM and is most similar to the HA concentrations in the softer gels. The 1.48 g/L PLL:8.52 g/L composition with at a charge ratio of 0.45 has a much higher HA concentration but has greater error because of the small amount of bulk complex coacervate layer that is recovered (∼1% by mass). We find that the complex coacervate phase makes up 0.8−5.6% by mass of the total solution with only 0.8% by mass of a complex coacervate phase

https://doi.org/10.1021/acspolymersau.3c00027
ACS Polym. Au 2024, 4, 109−119

existing at 250 mM at the charge ratio of 0.45 (see Figure S16 for more information). Generally, we find that in contrast to previously observed crowding effects, the critical ionic strength inside PAM gels appears to be lower than in the bulk solution.

To investigate the effect of uncrosslinked PAM on bulk solution complex coacervate behavior, 70 g/L linear PAM was added to the bulk HA and PLL solutions, and the resulting phases were investigated as a function of ionic strength (Figure 6b). Interestingly, after 24 h, the solutions remained cloudy except for the 250 and 300 mM ionic strength mixtures in which two distinct phases were formed. This prolonged cloudiness was not observed for sodium acetate solutions containing just HA and PLL. Using confocal microscopy, we confirmed that droplets of varying size distributions formed in the cloudy PAM, HA, and PLL mixtures. The addition of PAM seems to have a stabilizing effect on the complex coacervates even in solution. This could potentially be due to the viscoelastic nature of the solutions, since at 70 g/L, PAM is above the overlap concentration. With increasing ionic strength, the HA concentration in the complex coacervate phase decreases in all PLL/HA/PAM compositions (Figure 6b), but the phase remained stable even in [I] = 300 mM. Overall, the HA concentration in these droplets is less than the HA concentration in complex coacervate phases inside a gel. We note however that the samples in the solution study with linear PAM have not likely reached equilibrium after only 24 h, and a longer study is needed to fully understand the effect PAM has on complex coacervate phase behavior.

Modulus Effects

We find that the gel modulus can have interesting effects on complex coacervate droplets. There is an optimal modulus at which the PLL/HA phase has the greatest salt resistance. Figure 7a shows the critical ionic strength, defined as the soaking solution ionic strength required for the dissolution of complex coacervates as a function of the gel shear modulus. The critical ionic strength is highest for the 4.1 kPa gel at 270 mM, and lowest for ∼0.3 and 9.0−15 kPa gels at 180−190 mM. Interestingly, the optimum modulus of 4.1 kPa is comparable to the modulus of human spinal cord and gray matter with an average modulus around 3 kPa[64] and strikingly similar to cytosol modulus of 0.5−4 kPa.[65−67]

Figure 7a resembles typical complex coacervate phase diagrams. Underneath the curve, the complex coacervate phase is stable. Above the curve, PLL and HA are homogeneously distributed in the network. To further understand the gel effects on the phase behavior, it is important to note that the modulus of a gel is directly related to the polyacrylamide concentration. As the gel is more cross-linked, the modulus increases in equilibrium swelling conditions. The gel shear modulus scales quadratically with concentration, as predicted from Flory−Rehner theories in equilibrium.[68−70] Largely, this relationship is from the entropy loss of the network chains resulting from solvent swelling.[71] The gel modulus is predicted to be

$$G' = \frac{k_B T}{v_1}(1/2 - \chi)\phi_e^2 \quad (2)$$

where k_B is the Boltzmann constant, T is the absolute temperature, v_1 is the molar reference volume typically chosen as the molar segment volume, χ is Flory−Huggins interaction parameter, and ϕ_e is the equilibrium volume fraction that relates the internal pressure highly swollen gel in equilibrium

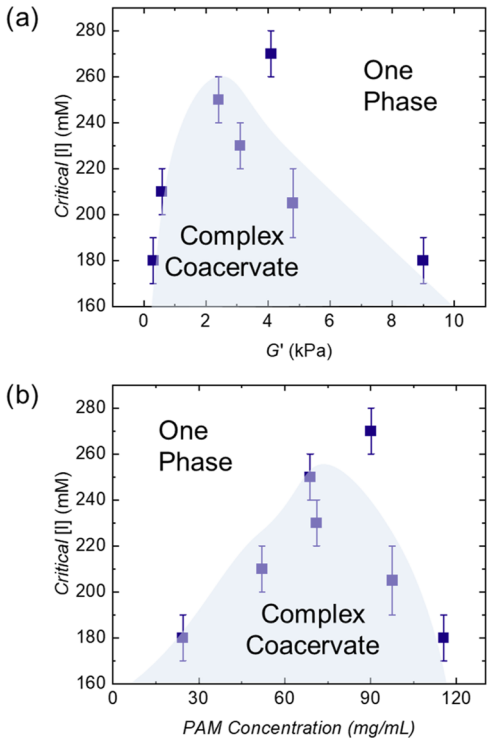

Figure 7. (a) Critical ionic strength as a function of the gel shear modulus. (b) Critical ionic strength as a function of the gel polyacrylamide concentration. The gel polyacrylamide concentrations were extrapolated using a quadratic relationship, $c_e = (G'/0.51)^{1/2}$, between the modulus and PAM concentration except for the moduli of 0.6, 3.1, and 9 kPa, where the PAM concentration was measured using dry and hydrated gel mass. Error bars for the critical ionic strength represent the steps in the increase of ionic strength that were used to reach the critical ionic strength. Error bars from the standard deviation of rheological measurements are too small to be seen. The shaded regions in both graphs indicate the region where complex coacervates exist and serves as just a guide to the eye.

to the shear modulus.[72] We plot the PAM concentration against the critical ionic strength in Figure 7b as a more typical phase diagram. In this way, the local gel concentration can be used to control the complex coacervate phase behavior in addition to the droplet size. For example, outside of equilibrium swelling, the gel can be concentrated by drying to either force complex coacervation or dissolution of PLL/HA. Near the critical point, any small changes in the gel network modulus as a function of ionic strength and swelling can have dramatic effects on the polyelectrolyte concentration in the complex coacervate phase, which we observe when measuring the HA concentration in the droplets in 2.4 and 3.1 kPa gels.

We can interpret the phase diagrams shown in Figure 7 as a balance of energies. The phase boundary is determined by the equilibrium of the translational entropy of all of the molecules (water and polyelectrolytes), gel strand entropic elasticity, and enthalpy (including electrostatic effects and excluded volume interaction between the gel and the polyelectrolytes). Therefore, the equilibrium describes that at a certain salt concentration and gel modulus the complex coacervate phase has a thermodynamic drive for formation. The salt stability is lower in the gel than in the bulk because the gel has to deform to create the droplets, which causes an energy penalty to complex coacervation. When there is a thermodynamic drive

https://doi.org/10.1021/acspolymersau.3c00027
ACS Polym. Au 2024, 4, 109−119

for complex coacervation, there is an equilibrium between two phases, the complex coacervate phase and the dilute phase, within the network. As complexation occurs, the gel deforms, and the amount of deformation is determined by the local modulus of the network and the phase diagram in Figure 7.

This balance in opposing pressures explains other observations, including that the volume of the droplets decreases inversely with the modulus and the change in the droplet radius is largest in softer gels. As shown in Figure 5a, the complex coacervate radius decreases with increasing ionic strength. This decrease in radius may be caused by a balance between the stress of complex coacervation on the network, σ_c, at a certain ionic strength, and the deformation of the gel. Complex coacervation stress depends only on the ionic strength of the system, and the gel modulus remains constant as a function of ionic strength. With increasing ionic strength, complex coacervation stress decreases, and the deformation in the network must be lower for the same gel modulus according to a simple balance:

$$G'\frac{\Delta V}{V} = -\Delta\sigma_c \tag{3}$$

where V is the initial volume of the complex coacervate. Comparing the radii of the 0.3 and 0.6 kPa at 100 and 180 mM gel, we find a constant change in σ_c of ca. −285 Pa for both gels. This relationship is also likely true for the higher-modulus gels; however, because the expected change in radius is smaller than the instrument resolution, the size appears to be stable. Also to note in this study, we are changing both the complex coacervate concentration and the gel network modulus, and that the gel is not homogeneously uniform in concentration.

With increasing concentration of the network and shear modulus, the PAM concentration increases quadratically, which likely contributes to the phase behavior shown in Figure 7. From these experiments, however, how the PAM network is involved in the droplet formation remains unclear, since the droplets are much larger than the network mesh size. Using G', the mesh size of the gel can be estimated with $G' = \frac{k_B T}{\xi^3}$. The softest gel in this study, G' = 0.039 kPa, has a mesh size of 47 nm and the stiffest gel in this study, G' = 15 kPa, has a mesh size of 6 nm (Table 1). The complex coacervate droplets are orders of magnitude larger than the mesh size of the gels, while the polymers forming the complex coacervates are only ∼1 nm and smaller than the mesh size. The gel modulus and droplet radius relationship is not consistent with cavitation theory as the gel modulus scales with radius to the −0.3 power.[58,59] This result is consistent with the balance of bulk gel deformation and coacervation pressure, which is expected in the case of a low surface tension (eq 3). In addition, the gel concentration influences the internal phase behavior of the complex coacervates, which makes this system more complex than simple cavitation. Even in solution, PAM seems to help stabilize the phase boundary, so the droplets likely have a very small surface tension that may not be large enough to cavitate.[73−76] Overall, PAM interacts with the complex coacervate phase. One important question that arises is: does the network get pushed aside out of the droplet, or does the network participate in the phase behavior, from either extension or compression of the network locally? These questions introduce new possibilities for understanding how the network may or may not participate in the droplet phase behavior.

Overall, this study shows that the complex coacervate droplet radius, phase, and concentration can be tuned by changing the local elasticity and concentration of the surrounding network. In loose networks, the PLL/HA complex coacervate phase droplet radius is large, polyelectrolyte concentration varies little from bulk conditions, and phase separation is suppressed in high ionic strength environments. In tighter networks, droplet radius is the smallest and polyelectrolyte concentration is high, but phase separation is suppressed in high ionic strength environments. However, in intermediate networks, there is much more ionic strength resistance and intermediate size droplets.

CONCLUSIONS

We have determined the size scale and phase behavior of poly-L-lysine and sodium hyaluronate complex coacervate phases in polyacrylamide gel networks. Using bright-field and confocal microscopies, we find that the modulus of the elastic environment of the complex coacervate phase impacts the shape, size, and salt resistance of the complex coacervate phase. The complex coacervates form stable, spherical droplets in these networks, and their volume is inversely proportional to the modulus. With increasing gel modulus, we find that the polyelectrolyte concentration increases and that the salt resistance of the complex coacervate droplets is nonmonotonic. The effects are optimized in ∼4 kPa gels, where the complex coacervate droplets have the most salt resistance. This study is the first to observe that the network impacts not only the size of bioinspired liquid phase separation but also the phase behavior, and opens new questions about possible mechanisms of how the network may participate in controlling liquid−liquid phase separation.

ASSOCIATED CONTENT

Supporting Information

The Supporting Information is available free of charge at https://pubs.acs.org/doi/10.1021/acspolymersau.3c00027.

More details on the formation of the complex coacervate droplets in varying-modulus gels; calibration curves; rheology data, time study, pH study, solution study; and images and histograms of bright-field and confocal microscopy results (PDF)

AUTHOR INFORMATION

Corresponding Author

Svetlana Morozova − *Department of Macromolecular Science and Engineering, Case Western Reserve University, Cleveland, Ohio 44106, United States;* orcid.org/0000-0002-1002-7413; Email: svetlana.morozova@case.edu

Authors

Kathryn G. Wilcox − *Department of Macromolecular Science and Engineering, Case Western Reserve University, Cleveland, Ohio 44106, United States*

Kai R. Yamagami − *Department of Macromolecular Science and Engineering, Case Western Reserve University, Cleveland, Ohio 44106, United States*

Brittany K. Roopnarine − *Department of Macromolecular Science and Engineering, Case Western Reserve University, Cleveland, Ohio 44106, United States;* orcid.org/0009-0005-8745-1297

Adam Linscott − *Department of Macromolecular Science and Engineering, Case Western Reserve University, Cleveland, Ohio 44106, United States*

Complete contact information is available at: https://pubs.acs.org/10.1021/acspolymersau.3c00027

Author Contributions

The manuscript was written through contributions of all authors. All authors have given approval to the final version of the manuscript. Credit: **Kai R. Yamagami** for formal analysis, investigation, methodology, writing-review & editing; Kathryn G. Wilcox for formal analysis, investigation, methodology, writing-review & editing; **Adam Linscott** formal analysis, investigation, writing-review & editing; Brittany Roopnarine for imaging and editing; Svetlana Morozova for project leadership, methodology, writing-review, & editing.

Funding

National Science Foundation and Case Western Reserve University.

Notes

The authors declare no competing financial interest.

■ ACKNOWLEDGMENTS

This material is based upon work supported by the National Science Foundation Graduate Research Fellowship under Grant No. 1937968. The authors thank Case Western Reserve University's Support of Undergraduate Research & Creative Endeavors−Arts, Humanities, and Social Sciences Program for funding. They also thank Sujata Dhakal for helping take confocal microscopy images for two solution study experiments, and Maite Rey for some of the initial work that led to this study.

■ ABBREVIATIONS

PLL, poly-L-Lysine hydrobromide; HA, sodium hyaluronate; PEG, polyethylene glycol; PAM, polyacrylamide

■ REFERENCES

(1) Minton, A. P. Excluded Volume as a Determinant of Macromolecular Structure and Reactivity. *Biopolymers* **1981**, *20* (10), 2093−2120.
(2) Fulton, A. B. How Crowded Is the Cytoplasm? *Cell* **1982**, *30* (2), 345−347.
(3) Zimmerman, S. B.; Trach, S. O. Estimation of Macromolecule Concentrations and Excluded Volume Effects for the Cytoplasm of Escherichia Coli. *J. Mol. Biol.* **1991**, *222* (3), 599−620.
(4) André, A. A. M.; Spruijt, E. Liquid−Liquid Phase Separation in Crowded Environments. *Int. J. Mol.* **2020**, *21* (16), No. 5908, DOI: 10.3390/ijms21165908.
(5) Brangwynne, C. P.; Tompa, P.; Pappu, R. V. Polymer Physics of Intracellular Phase Transitions. *Nat. Phys.* **2015**, *11* (11), 899−904.
(6) Zhao, H.; Ibrahimova, V.; Garanger, E.; Lecommandoux, S. Dynamic Spatial Formation and Distribution of Intrinsically Disordered Protein Droplets in Macromolecularly Crowded Protocells. *Angew. Chem., Int. Ed.* **2020**, *59* (27), 11028−11036.
(7) Blocher, W. C.; Perry, S. L. Complex Coacervate-Based Materials for Biomedicine. *WIREs Nanomed. Nanobiotechnol.* **2017**, *9* (4), No. e1442.
(8) Blocher McTigue, W. C.; Perry, S. L. Design Rules for Encapsulating Proteins into Complex Coacervates. *Soft Matter* **2019**, *15* (15), 3089−3103.
(9) Sing, C. E.; Perry, S. L. Recent Progress in the Science of Complex Coacervation. *Soft Matter* **2020**, *16* (12), 2885−2914.
(10) Rumyantsev, A. M.; Jackson, N. E.; De Pablo, J. J. Polyelectrolyte Complex Coacervates: Recent Developments and New Frontiers. *Ann. Rev. Condens. Matter Phys.* **2021**, *12*, 155−176.
(11) Nakashima, K. K.; André, A. A. M.; Spruijt, E. Enzymatic Control over Coacervation. *Methods Enzymol.* **2021**, *646*, 353−389.
(12) Yewdall, N. A.; André, A. A. M.; Lu, T.; Spruijt, E. Coacervates as Models of Membraneless Organelles. *Curr. Opin. Colloid Interface Sci.* **2021**, *52*, No. 101416.
(13) Gao, N.; Mann, S. Membranized Coacervate Microdroplets: From Versatile Protocell Models to Cytomimetic Materials. *Acc. Chem. Res.* **2023**, *56* (3), 297−307.
(14) Wu, H.; Qiao, Y. Engineering Coacervate Droplets towards the Building of Multiplex Biomimetic Protocells. *Supramol. Mater.* **2022**, *1*, No. 100019.
(15) Cook, A. B.; Novosedlik, S.; van Hest, J. C. M. Complex Coacervate Materials as Artificial Cells. *Acc. Mater. Res.* **2023**, *4* (3), 287−298.
(16) Yin, Z.; Tian, L.; Patil, A. J.; Li, M.; Mann, S.; Yin, Z.; Patil, A. J.; Li, M.; Mann, S.; Tian, L. Spontaneous Membranization in a Silk-Based Coacervate Protocell Model. *Angew. Chem.* **2022**, *134* (17), No. e202202302.
(17) Black, K. A.; Priftis, D.; Perry, S. L.; Yip, J.; Byun, W. Y.; Tirrell, M. Protein Encapsulation via Polypeptide Complex Coacervation. *ACS Macro Lett.* **2014**, *3* (10), 1088−1091.
(18) Pir Cakmak, F.; Grigas, A. T.; Keating, C. D. Lipid Vesicle-Coated Complex Coacervates. *Langmuir* **2019**, *35* (24), 7830−7840.
(19) Deshpande, S.; Brandenburg, F.; Lau, A.; Last, M. G. F.; Spoelstra, W. K.; Reese, L.; Wunnava, S.; Dogterom, M.; Dekker, C. Spatiotemporal Control of Coacervate Formation within Liposomes. *Nat. Commun.* **2019**, *10* (1), No. 1800, DOI: 10.1038/s41467-019-09855-x.
(20) Jang, Y.; Hsieh, M. C.; Dautel, D.; Guo, S.; Grover, M. A.; Champion, J. A. Understanding the Coacervate-to-Vesicle Transition of Globular Fusion Proteins to Engineer Protein Vesicle Size and Membrane Heterogeneity. *Biomacromolecules* **2019**, *20* (9), 3494−3503.
(21) Kizilay, E.; Dinsmore, A. D.; Hoagland, D. A.; Sun, L.; Dubin, P. L. Evolution of Hierarchical Structures in Polyelectrolyte−Micelle Coacervates. *Soft Matter* **2013**, *9* (30), 7320−7332.
(22) Li, L.; Srivastava, S.; Andreev, M.; Marciel, A. B.; De Pablo, J. J.; Tirrell, M. V. Phase Behavior and Salt Partitioning in Polyelectrolyte Complex Coacervates. *Macromolecules* **2018**, *51* (8), 2988−2995.
(23) Radhakrishna, M.; Basu, K.; Liu, Y.; Shamsi, R.; Perry, S. L.; Sing, C. E. Molecular Connectivity and Correlation Effects on Polymer Coacervation. *Macromolecules* **2017**, *50* (7), 3030−3037.
(24) Knoerdel, A. R.; McTigue, W. C. B.; Sing, C. E. Transfer Matrix Model of PH Effects in Polymeric Complex Coacervation. *J. Phys. Chem. B* **2021**, *125* (31), 8965−8980, DOI: 10.1021/ACS.JPCB.1C03065.
(25) Neitzel, A. E.; Fang, Y. N.; Yu, B.; Rumyantsev, A. M.; De Pablo, J. J.; Tirrell, M. V. Polyelectrolyte Complex Coacervation across a Broad Range of Charge Densities. *Macromolecules* **2021**, *54* (14), 6878−6890, DOI: 10.1021/acs.macromol.1c00703.
(26) Dinic, J.; Marciel, A. B.; Tirrell, M. V. Polyampholyte Physics: Liquid−Liquid Phase Separation and Biological Condensates. *Curr. Opin. Colloid Interface Sci.* **2021**, *54*, No. 101457.
(27) Lytle, T. K.; Chang, L. W.; Markiewicz, N.; Perry, S. L.; Sing, C. E. Designing Electrostatic Interactions via Polyelectrolyte Monomer Sequence. *ACS Cent. Sci.* **2019**, *5* (4), 709−718, DOI: 10.1021/acscentsci.9b00087.
(28) Zhang, Y.; Cremer, P. S. Interactions between Macromolecules and Ions: The Hofmeister Series. *Curr. Opin. Chem. Biol.* **2006**, *10* (6), 658−663.
(29) Iyer, D.; Syed, V. M. S.; Srivastava, S. Influence of Divalent Ions on Composition and Viscoelasticity of Polyelectrolyte Complexes. *J. Polym. Sci.* **2021**, *59* (22), 2895−2904.
(30) Lytle, T. K.; Sing, C. E. Tuning Chain Interaction Entropy in Complex Coacervation Using Polymer Stiffness, Architecture, and Salt Valency. *Mol. Syst. Des. Eng.* **2018**, *3* (1), 183−196.

(31) Wang, Q.; Schlenoff, J. B. The Polyelectrolyte Complex/Coacervate Continuum. *Macromolecules* **2014**, *47* (9), 3108−3116, DOI: 10.1021/ma500500q.
(32) Schlenoff, J. B.; Yang, M.; Digby, Z. A.; Wang, Q. Ion Content of Polyelectrolyte Complex Coacervates and the Donnan Equilibrium. *Macromolecules* **2019**, *52* (23), 9149−9159, DOI: 10.1021/acs.macromol.9b01755.
(33) Kayitmazer, A. B.; Koksal, A. F.; Iyilik, E. K. Complex Coacervation of Hyaluronic Acid and Chitosan: Effects of PH, Ionic Strength, Charge Density, Chain Length and the Charge Ratio. *Soft Matter* **2015**, *11* (44), 8605−8612, DOI: 10.1039/C5SM01829C.
(34) Overbeek, J. T.; Voorn, M. J. Phase Separation in Polyelectrolyte Solutions. Theory of Complex Coacervation. *J. Cell. Comp. Physiol.* **1957**, *49* (S1), 7−26.
(35) Crowe, C. D.; Keating, C. D. Liquid−Liquid Phase Separation in Artificial Cells. *Interface Focus* **2018**, *8*, No. 20180032.
(36) Perry, S. L. Phase Separation: Bridging Polymer Physics and Biology. *Curr. Opin. Colloid Interface Sci.* **2019**, *39*, 86−97.
(37) Park, S.; Barnes, R.; Lin, Y.; Jeon, B.-j.; Najafi, S.; Delaney, K. T.; Fredrickson, G. H.; Shea, J. E.; Hwang, D. S.; Han, S. Dehydration Entropy Drives Liquid-Liquid Phase Separation by Molecular Crowding. *Commun. Chem.* **2020**, *3* (1), No. 83, DOI: 10.1038/s42004-020-0328-8.
(38) Lytle, T. K.; Salazar, A. J.; Sing, C. E. Interfacial Properties of Polymeric Complex Coacervates from Simulation and Theory. *J. Chem. Phys.* **2018**, *149* (16), No. 163315, DOI: 10.1063/1.5029934.
(39) Marianelli, A. M.; Miller, B. M.; Keating, C. D. Impact of Macromolecular Crowding on RNA/Spermine Complex Coacervation and Oligonucleotide Compartmentalization. *Soft Matter* **2018**, *14* (3), 368−378.
(40) Lemetti, L.; Hirvonen, S. P.; Fedorov, D.; Batys, P.; Sammalkorpi, M.; Tenhu, H.; Linder, M. B.; Aranko, A. S. Molecular Crowding Facilitates Assembly of Spidroin-like Proteins through Phase Separation. *Eur. Polym. J.* **2019**, *112*, 539−546.
(41) Gao, S.; Srivastava, S. Comb Polyelectrolytes Stabilize Complex Coacervate Microdroplet Dispersions. *ACS Macro Lett.* **2022**, *11* (7), 902−909, DOI: 10.1021/acsmacrolett.2c00327.
(42) Gao, S.; Holkar, A.; Srivastava, S. Protein−Polyelectrolyte Complexes and Micellar Assemblies. *Polymers* **2019**, *11* (7), No. 1097, DOI: 10.3390/polym11071097.
(43) Mctigue, W. C. B.; Perry, S. L.; Mctigue, W. C. B.; Perry, S. L. Protein Encapsulation Using Complex Coacervates: What Nature Has to Teach Us. *Small* **2020**, *16* (27), No. 1907671.
(44) Srivastava, S.; Andreev, M.; Levi, A. E.; Goldfeld, D. J.; Mao, J.; Heller, W. T.; Prabhu, V. M.; De Pablo, J. J.; Tirrell, M. V. Gel Phase Formation in Dilute Triblock Copolyelectrolyte Complexes. *Nat. Commun.* **2017**, *8* (1), No. 14131, DOI: 10.1038/ncomms14131.
(45) Srivastava, S.; Levi, A. E.; Goldfeld, D. J.; Tirrell, M. V. Structure, Morphology, and Rheology of Polyelectrolyte Complex Hydrogels Formed by Self-Assembly of Oppositely Charged Triblock Polyelectrolytes. *Macromolecules* **2020**, *53* (14), 5763−5774, DOI: 10.1021/acs.macromol.0c00847.
(46) Bai, Q.; Chen, X.; Chen, J.; Liu, Z.; Lin, Y. N.; Yang, S.; Liang, D. Morphology and Dynamics of Coexisting Phases in Coacervate Solely Controlled by Crowded Environment. *ACS Macro Lett.* **2022**, *11* (9), 1107−1111, DOI: 10.1021/acsmacrolett.2c00409.
(47) Feric, M.; Vaidya, N.; Harmon, T. S.; Mitrea, D. M.; Zhu, L.; Richardson, T. M.; Kriwacki, R. W.; Pappu, R. V.; Brangwynne, C. P. Coexisting Liquid Phases Underlie Nucleolar Subcompartments. *Cell* **2016**, *165* (7), 1686−1697.
(48) Banani, S. F.; Lee, H. O.; Hyman, A. A.; Rosen, M. K. Biomolecular Condensates: Organizers of Cellular Biochemistry. *Nat. Rev. Mol. Cell Biol.* **2017**, *18* (5), 285−298.
(49) Brangwynne, C. P.; Eckmann, C. R.; Courson, D. S.; Rybarska, A.; Hoege, C.; Gharakhani, J.; Jülicher, F.; Hyman, A. A. Germline P Granules Are Liquid Droplets That Localize by Controlled Dissolution/Condensation. *Science* **2009**, *324* (5935), 1729−1732.
(50) Brangwynne, C. P. Soft Active Aggregates: Mechanics, Dynamics and Self-Assembly of Liquid-like Intracellular Protein Bodies. *Soft Matter* **2011**, *7* (7), 3052−3059.
(51) Böddeker, T. J.; Rosowski, K. A.; Berchtold, D.; Emmanouilidis, L.; Han, Y.; Allain, F. H. T.; Style, R. W.; Pelkmans, L.; Dufresne, E. R. Non-Specific Adhesive Forces between Filaments and Membraneless Organelles. *Nat. Phys.* **2022**, *18* (5), 571−578.
(52) Fernández-Rico, C.; Sai, T.; Sicher, A.; Style, R. W.; Dufresne, E. R. Putting the Squeeze on Phase Separation. *JACS Au* **2022**, *2* (1), 66−73, DOI: 10.1021/jacsau.1c00443.
(53) Style, R. W.; Sai, T.; Fanelli, N.; Ijavi, M.; Smith-Mannschott, K.; Xu, Q.; Wilen, L. A.; Dufresne, E. R. Liquid-Liquid Phase Separation in an Elastic Network. *Phys. Rev. X* **2018**, *8*, No. 011028, DOI: 10.1103/physrevx.8.011028.
(54) Hutchens, S. B.; Fakhouri, S.; Crosby, A. J. Elastic Cavitation and Fracture via Injection. *Soft Matter* **2016**, *12* (9), 2557−2566.
(55) Henzel, T.; Nijjer, J.; Chockalingam, S.; Wahdat, H.; Crosby, A. J.; Yan, J.; Cohen, T. Interfacial Cavitation. *PNAS Nexus* **2022**, *1* (4), No. pgac217, DOI: 10.1093/pnasnexus/pgac217.
(56) Barney, C. W.; Dougan, C. E.; McLeod, K. R.; Kazemi-Moridani, A.; Zheng, Y.; Ye, Z.; Tiwari, S.; Sacligil, I.; Riggleman, R. A.; Cai, S.; Lee, J. H.; Peyton, S. R.; Tew, G. N.; Crosby, A. J. Cavitation in Soft Matter. *Proc. Natl. Acad. Sci. U.S.A.* **2020**, *117* (17), 9157−9165.
(57) Kundu, S.; Crosby, A. J. Cavitation and Fracture Behavior of Polyacrylamide Hydrogels. *Soft Matter* **2009**, *5* (20), 3963−3968.
(58) Rosowski, K. A.; Sai, T.; Vidal-Henriquez, E.; Zwicker, D.; Style, R. W.; Dufresne, E. R. Elastic Ripening and Inhibition of Liquid−Liquid Phase Separation. *Nat. Phys.* **2020**, *16* (4), 422−425.
(59) Rosowski, K. A.; Vidal-Henriquez, E.; Zwicker, D.; Style, R. W.; Dufresne, E. R. Elastic Stresses Reverse Ostwald Ripening. *Soft Matter* **2020**, *16* (25), 5892−5897.
(60) Kim, J. Y.; Liu, Z.; Weon, B. M.; Cohen, T.; Hui, C. Y.; Dufresne, E. R.; Style, R. W. Extreme Cavity Expansion in Soft Solids: Damage without Fracture. *Sci. Adv.* **2020**, *6* (13), No. eaaz0418, DOI: 10.1126/sciadv.aaz0418.
(61) Liu, J. X.; Haataja, M. P.; Košmrlj, A.; Datta, S. S.; Arnold, C. B.; Priestley, R. D. Liquid−Liquid Phase Separation within Fibrillar Networks. *Nat. Commun.* **2023**, *14* (1), No. 6085, DOI: 10.1038/s41467-023-41528-8.
(62) Biswas, S.; Mukherjee, B.; Chakrabarti, B. Thermodynamics Predicts a Stable Microdroplet Phase in Polymer−Gel Mixtures Undergoing Elastic Phase Separation. *Soft Matter* **2022**, *18* (42), 8117−8123.
(63) Sheth, S.; Jain, E.; Karadaghy, A.; Syed, S.; Stevenson, H.; Zustiak, S. P. UV Dose Governs UV-Polymerized Polyacrylamide Hydrogel Modulus. *Int. J. Polym. Sci.* **2017**, *2017*, No. 5147482, DOI: 10.1155/2017/5147482.
(64) McKee, C. T.; Last, J. A.; Russell, P.; Murphy, C. J. Indentation Versus Tensile Measurements of Young's Modulus for Soft Biological Tissues. *Tissue Eng., Part B* **2011**, *17* (3), No. 155, DOI: 10.1089/ten.teb.2010.0520.
(65) Chen, J.; Irianto, J.; Inamdar, S.; Pravincumar, P.; Lee, D. A.; Bader, D. L.; Knight, M. M. Cell Mechanics, Structure, and Function Are Regulated by the Stiffness of the Three-Dimensional Microenvironment. *Biophys. J.* **2012**, *103* (6), 1188.
(66) Slomka, N.; Oomens, C. W. J.; Gefen, A. Evaluating the Effective Shear Modulus of the Cytoplasm in Cultured Myoblasts Subjected to Compression Using an Inverse Finite Element Method. *J. Mech. Behav. Biomed. Mater.* **2011**, *4* (7), 1559−1566.
(67) Ofek, G.; Natoli, R. M.; Athanasiou, K. A. In Situ Mechanical Properties of the Chondrocyte Cytoplasm and Nucleus. *J. Biomech.* **2009**, *42* (7), 873−877.
(68) Barrat, J. L.; Joanny, J. F. Persistence Length of Polyelectrolyte Chains. *Europhys. Lett.* **1993**, *24* (5), 333−338.
(69) Morozova, S.; Muthukumar, M. Elasticity at Swelling Equilibrium of Ultrasoft Polyelectrolyte Gels: Comparisons of Theory and Experiments. *Macromolecules* **2017**, *50* (6), 2456−2466.

(70) Flory, P. J.; Rehner, J. Statistical Mechanics of Cross-Linked Polymer Networks I. Rubberlike Elasticity. *J. Chem. Phys.* **1943**, *11* (11), 512−520.
(71) Wilcox, K. G.; Kozawa, S. K.; Morozova, S. Fundamentals and Mechanics of Polyelectrolyte Gels: Thermodynamics, Swelling, Scattering, and Elasticity. *Chem. Phys. Rev.* **2021**, *2* (4), No. 041309.
(72) Horkay, F.; Nishi, K.; Shibayama, M. Decisive Test of the Ideal Behavior of Tetra-PEG Gels. *J. Chem. Phys.* **2017**, *146* (16), No. 164905.
(73) Priftis, D.; Farina, R.; Tirrell, M. Interfacial Energy of Polypeptide Complex Coacervates Measured via Capillary Adhesion. *Langmuir* **2012**, *28* (23), 8721−8729.
(74) Spruijt, E.; Sprakel, J.; Stuart, M. A. C.; Van Der Gucht, J. Interfacial Tension between a Complex Coacervate Phase and Its Coexisting Aqueous Phase. *Soft Matter* **2010**, *6* (1), 172−178, DOI: 10.1039/B911541B.
(75) Prabhu, V. M. Interfacial Tension in Polyelectrolyte Systems Exhibiting Associative Liquid−Liquid Phase Separation. *Curr. Opin. Colloid Interface Sci.* **2021**, *53*, No. 101422.
(76) Jho, Y. S.; Yoo, H. Y.; Lin, Y.; Han, S.; Hwang, D. S. Molecular and Structural Basis of Low Interfacial Energy of Complex Coacervates in Water. *Adv. Colloid Interface Sci.* **2017**, *239*, 61−73.

https://doi.org/10.1021/acspolymersau.3c00027
ACS Polym. Au 2024, 4, 109−119